Leaf vein topology confers water transport efficiency

Amy Ny Aina ARITSARA
Guangxi University
Ming-Yuan NI
Youjiang Medical University for Nationalities https://orcid.org/0000-0001-8789-274X
Tahiana RAMANANANTOANDRO
University of Antananarivo https://orcid.org/0000-0001-5080-7118
Shi-Dan ZHU
Guangxi University https://orcid.org/0000-0002-9228-368X
You-Zhi LI
Guangxi University https://orcid.org/0000-0001-8841-2795
Sean GLEASON
USDA-ARS https://orcid.org/0000-0002-5607-4741
Lawren SACK
University of California https://orcid.org/0000-0002-7009-7202
Kun-Fang CAO (kunfangcao@gxu.edu.cn)
Guangxi University https://orcid.org/0000-0002-2253-7189

Research Article

Keywords: Leaf vein topology, minor veins, leaf mass per area, extraxylary water transport pathway, stomatal conductance, non-vein area

Posted Date: December 6th, 2022

DOI: https://doi.org/10.21203/rs.3.rs-2344990/v1

Abstract

The evolution of xylem vessels and dense leaf vein networks in flowering plants enabled unprecedented increases in plant water transport and rates of CO_2 assimilation. We tested the hypothesis that independent of vein density, higher leaf vein topological efficiency (*VTE*), achieved with denser free vein endings, would reduce the extraxylary pathlength, further benefitting whole-leaf conductance, while reducing carbon investment, and releasing space for light capture. Our analysis across 52 phylogenetically diverse angiosperm species demonstrated that for a given vein density, high *VTE* conferred by dense free endings can shorten the extraxylary pathlength by up to 11%. Across species, high *VTE* was associated with high stomatal conductance, non-vein area fraction for light capture, and low leaf mass per area. Our findings identify leaf vein topological efficiency as an important measure of the use of leaf space and biomass, and a key factor influencing plant adaptation to historical and future environmental conditions.

Introduction

In land plants, leaves are the main sites of carbon fixation and biomass production, and these functions require hundreds of water molecules be transported to the leaf surface to fix a single molecule of CO_2. Yet, the pathlength between the soil and stomata remains a strong hydraulic resistance that must be overcome to maintain leaf irrigation, transpiration, and photosynthesis [1–3]. Thus, natural selection has favored the evolution of high-capacity transport, including efficient networks of xylem vessels, which contribute to organ and whole plant hydraulic conductance, especially in productive habitats [4–6]. A particularly strong bottleneck arises in the very terminus of the hydraulic network, when water exits the xylem conduits, crosses the bundle sheath cells, and traverses the leaf mesophyll to the sites of evaporation and photosynthesis [7]. This short “extraxylary” pathway – through the root cortex and the leaf mesophyll – can account for up to 70 to 90 percent of the total plant hydraulic resistance [8–11]. In leaves, shortening this pathway by dense vasculature substantially reduces the leaf hydraulic resistance [12], but increases the leaf xylem construction cost [13,14]. Therefore, natural selection should favor a specific venation design to achieve the highest hydraulic conductance and photosynthesis per unit carbon invested [1,14,15]. As the smallest veins in the leaf—the “minor veins”—constitute the bulk of the vein length, they should be arranged to minimize the extraxylary pathlength resistance per unit vein length [16]. We aimed to identify vein topology that reduces the extraxylary pathlength and leaf biomass investment, increases photosynthetic gases uptake efficiency, and consequently leads to high physiological performance.

The role of optimizing vein topology may be especially important in species that already evolved high vein density. During the Cretaceous, the radiation and increasing dominance of angiosperms entailed, and may have been enabled by, dramatic increases in the length of vein per unit leaf area (hereafter “vein density”; *VD*), thus drove increases in hydraulic conductance and allowed high photosynthetic rates [17,18]. However, since ca. 120 Mya the evolution of high *VD* slowed in most angiosperm lineages, suggesting

that increasing *VD* provided diminishing returns in fitness [17], a hypothesis supported by experiments showing that increases in *VD* had a saturating effect on hydraulic conductance in artificial leaves of a given thickness [16]. Further, a study of phylogenetically and ecologically diverse species found that the optimal vein density should match the distance between veins with the vertical distance from vein to the evaporative surface; as such, for a given vein to evaporative distance, further increase in *VD*, would not lead to proportional hydraulic efficiency [18]. In addition to providing diminishing returns in benefits, a high *VD* necessitates additional costs in space and biomass investment: while minor veins contribute less than 5% of the total leaf biomass [19], and do not meaningfully contribute to the leaf mass per area (*LMA*) [20], the metabolic and construction costs of their thick-walled conduits and associated bundle sheaths may be substantial [14]. Further, high vein density involves the displacement of photosynthetic tissues [21].

Yet, independent of *VD*, shifts in vein topology may shorten the extraxylary pathlength distance and thereby confer a higher transport efficiency contributing to gas exchange capacity and productivity. Such a benefit for characterizing vein topology would be in addition to those previously associated vein "loopiness", i.e., the amount of connectivity per leaf area, focused on its benefits for redundancy of the network architecture, and potential for contributing tolerance against drought or freezing-induced xylem embolism, mechanical damage or herbivory [12,22].

Notably, previous studies quantifying vein topology have focused on geometric parameters that did not completely isolate vein topological efficiency from *VD* [12,23,24]. We developed an approach to disentangle vein topology from *VD* by quantifying the relative benefit (extraxylary pathlength shortening) independent of vein length and projected area. We tested the hypothesis that angiosperms gradually acquired optimized vein topology, which also entails a greater space allocation to photosynthetic mesophyll, and enables greater stomatal conductance and photosynthetic rate, and less expensive leaves.

Results

Contribution of free-ending veinlets and vein topological efficiency to stomatal conductance

Vein topological efficiency (*VTE*), i.e., the vein-to-abaxial epidermis distance for actual leaves relative to modeled leaves (gridded vein systems) of the same vein density (*VD*), varied from − 1.2% ± 0.3 (high loopiness) to 11.0% ± 1.2 (more free ending veins) (Fig. 1). *VTE* was independent of vein density (Figure S1), but exhibited modest to strong association with *FEV* density metrics, such that high *VTE* was largely driven by high *FEV* relative length (Fig. 2a, Figure S2, Figure S3). Additionally, species with high *VTE* possessed narrow minor vein diameter (Fig. 2b) and the vein topology-driven extraxylary pathlength reduction correlated with high stomatal conductance (Fig. 3a). A *VTE* of 11% was associated with 38-fold higher G_{smax} (1.30 $mol \cdot m^{-1} \cdot s^{-1}$) than VTE of 0%. In addition to the link between *VTE* and extraxylary pathlength, the *SEM* distinguished two other potential links between *VTE* and G_{smax}; either via *LMA* or *nVF* (Fig. 4), which were negatively or positively associated with G_{smax}, respectively (Figure S4).

Influence of VTE on biomass investment and leaf photosynthetic area

High *VTE* was also associated with low biomass investment on leaf and low space allocation to veins. *VTE* correlated positively with the *nVF* and negatively with leaf mass per area; a *VTE* of 11% was associated with 32% higher non-vein area fraction (a relative increase of 57%, Fig. 3b) and 140 g m^{-2} lower *LMA* (a relative decrease of 85%, Fig. 3c, Figure S5) compared to *VTE* of *0%*. The series of vein models with increasing *FEV* relative length demonstrated that the contribution of *FEVs* alone would not explain the observed gain in *nVF* with increasing *VTE* (Fig. 3b,d), unless the negative correlation between minor vein diameter and *VTE* was added to the model (Fig. 3b,e). Minor vein diameter reduction with increasing *VTE* resulted in similar slope between the modelled and the observed *nVF*, with approximately 10% *nVF* remaining unexplained.

Vein topological efficiency and safety trade-off

However, *VTE* was strongly correlated with vein geometrical metrics that mainly characterize vein redundancy: high *VTE* was associated with low vein loopiness, meshedness, areole circularity and high areole elongation ratio (Fig. 5). *VTE* was negatively correlated with leaf capacitance (C_1) for the pooled data from the two sites, and independent of turgor loss point (*TLP*) (Figure S6).

Discussion

We demonstrated that across diverse species, abundant free-ending veinlets increased vein topological efficiency. Then, independent of vein density, high vein topological efficiency was associated with short extraxylary pathlength between the xylem and the leaf surface, enabling high maximal stomatal conductance, large mesophyll volume, and low carbon investment in leaf construction.

For a given vein density, an efficient vein topology significantly shortened the diagonal distance between the vein and the abaxial leaf surface. *VTE* was independent of vein density, and unlike vein density showed no significant phylogenetic signal, suggesting that the optimization of vein topology is labile and responsive to selection pressure during the angiosperm radiation, i.e., within and across basally and recently derived clades. For a given vein density, leaves may shorten the extraxylary pathway by constructing highly ramified venation and developing more free-end veinlets (*FEVs*). The additional benefit of a high *FEV*s in conferring a high *VTE* beyond a high vein density extends the previous work on the importance of *FEV*s as a contributor to vein density [23]. Further, the role of vein topology in hydraulic flow extends its previously described importance in providing vein redundancy to confer hydraulic safety to disruption by damage or herbivory [25,26].

Our findings demonstrate that optimized vein topology similarly to high vein density can shorten the distance for water transport from xylem to the sites of evaporation, thus lowering the resistance to water transport across the mesophyll, and potentially increasing whole-leaf gas exchange. Across species, a high *VTE* in addition to a high *VD* was associated with high G_{smax}. Notably, while several studies have reported significant correlations between vein density, stomatal conductance and light saturated

photosynthetic rate across diverse species [27–30], while other studies have reported either weak or no correlation between these traits [31–33]. This implies the potential for decoupling between vein density and gas exchange, especially when considering species adapted across aridity gradients [34]. The plants in arid habitats are likely to exhibit contrasting soil-to-stomata pressure gradients (e.g., atmospheric vs soil aridity) as well as different stomatal responses to leaf water potential and vapor pressure deficit [35,36]. For plants considered in a given environment, the coordination between water supply (conductance) and demand (transpiration) is expected to maximize photosynthetic gas exchange, hence, the coordination between vein topology and stomatal conductance [30].

Our findings suggest that a major benefit of increasing *VTE* is the resulting increase of lamina area for photosynthetic light capture. The areole outside the veins has a dense and thick layer of palisade mesophyll tissue, where the vast majority of light capture and photosynthesis in eudicot leaves takes place [37], whereas the areas directly above the veins contain only a thin (or no) mesophyll layer and a few (or no) stomata. Compared to species with low *VTE*, species with high *VTE* had greater areole area fraction. However, *FEV*s alone did not suffice to explain the gain in *nVF* to the extent suggested by the correlation analyses, rather the negative scaling between minor vein diameter and *VTE* explained a large percentage of the *nVF* gain. Thus, the gain in *nVF* with increasing vein topological efficiency was largely driven by high *VTE* in species having thin minor veins. All else being equal, a high non-vein area fraction would contribute to a high photosynthetic rate and stomatal conductance per unit leaf area.

We demonstrated that high *VTE* was associated with low *LMA*. This finding suggests a co-selection of traits that would contribute to rapid gas exchange per leaf mass, i.e., high *VTE* and low *LMA*. Notably, increasing investment in *VD* or *FEV*s would not influence *LMA*; *VD* was statistically and mechanistically independent of *LMA* across over 350 angiosperm species [20], and this is consistent with the minor veins contributing only ca. 5% of the total leaf mass [19]. By contrast, several studies have reported significant correlations between *LMA* and other leaf traits, such as leaf and palisade mesophyll thickness [38,39], and John *et al.* (2017) identified the leaf thickness and tissue density (thick cell walls) as the strongest driver of *LMA*, and both can increase the resistance to gas diffusion across mesophyll, limiting carbon uptake and assimilation.

Our analysis of model vein systems with increasing *VTE* showed that high *VTE* was associated with low loopiness and meshedness, metrics proposed by Price & Weitz (2014), or high loop elongation and low loop circularity proposed by Blonder et al (2018). Functionally, “loopy” vein systems allow for alternate water transport pathways (hydraulic “redundancy”) in case of embolism or damage to part of the vein network [12,22]. Conversely, excessive development of *FEVs* – low redundancy – may weaken resistance of the leaf to hydraulic failure, mechanical damage (force to punch) and herbivory (tannins) [24–26]. Our finding that increasing *VTE* would increase hydraulic delivery from veins to epidermis suggests the possibility of a trade-off in vein topology with respect to its contributions to efficiency and safety. Yet, the link between *VTE* and leaf hydraulic safety is still controversial. In fact, low *VTE* (high redundancy) species were associated with large-diameter minor veins, which may host conduits with large diameter

that are more sensitive to implosion than narrow conduits [40], disrupting water conduction before embolism [41]. Plants with low *VTE* may compensate the vulnerability of large minor veins with high redundancy, leading to even high carbon investment in leaf veins. Further, *VTE* was weakly associated or independent of *TLP* which quantify the sensitivity of mesophyll cells during desiccation [42]. Thus, the relationship between leaf hydraulic safety and vein topology is likely variable, depending on the influence of many other leaf structural and water relation traits.

From the perspective of leaf construction, the correspondence of high *VTE* with low *LMA* is consistent with rapid resource acquisition, hence high G_{smax}, while the correspondence of low *VTE* with high *LMA* and high area-based capacitance would reinforce stress tolerance. High capacitance serves the maintain the leaf water potential at mild value and has been marginally associated with low leaf conductance [43]. In addition, leaves with high *LMA* and low G_{smax} are commonly interpreted as “tough” (thick and/or dense) leaves conferring long leaf lifespan, but also slow *leaf-mass-based* rates of photosynthesis, whereas high G_{smax} is generally aligned with fast *leaf-area-based* rates of water transport and photosynthesis [44,45]. Vein topological efficiency would thus contribute to the set of traits that are related to area-based and mass-based rates of gas exchange, and thus potentially plant productivity.

Overall, the contribution of vein topology to gas exchange rates (via G_{smax}) would arise from multiple pathways including water flow pathways, leaf carbon economics, and spatial allocation of the mesophyll.

Conclusion

We developed a novel approach to quantify the effect of leaf vein topology for water transport outside the xylem, and its association with key structural and physiological features of angiosperm species of both basal and more recent divergences. The methods require only a basic light microscope and camera. Vein topology varied across species, with abundant free-ending veinlets leading to high vein topology efficiency, and the latter being associated with high maximal stomatal conductance, large leaf volume available for photosynthetic tissues, and low *LMA*. The shortening of the extraxylary pathlength through optimization of vein topology could result in increased hydraulic efficiency and photosynthesis relative to leaf construction cost, evolving repeatedly and probably contributing to the success of angiosperms in competitive habitats.

Online Methods

Study site and species

We selected 52 phylogenetically and ecologically diverse angiosperm species varying strongly in leaf venation architecture and vein density (*VD*; Table S1, Figure S7). All the 52 species are hypostomatic. To ensure a wide range of *VD*, and to test evolutionary shifts in vein topology, we sampled two groups of species: a first set from basally divergent groups occurring in a moist tropical forest, which was expected

to have low *VD* [17,46], and a second set from more derived groups native to a water-limited karst habitat, expected to have high *VD* [34]. Thus, we sampled thirty magnoliid species (23 trees, five lianas and two herbs), including a “living fossil” angiosperm tree, *Takhtajania perrieri* [47], from the tropical montane forest of Anjanaharibe-Sud Natural Reserve in the Sava Region of Madagascar (14°44'29"S, 49°29'50"E), and 22 tree species from a subtropical evergreen-deciduous mixed karst forest in China (25°9’9”N, 108°2’23”E). The tropical montane forest grows between 875 m and 1950 m elevation, experiences mean monthly temperatures varying from 8.6 to 25.7°C, and receives 2000 to 3600 mm of annual precipitation [48,49]. The subtropical forest grows between 410 m and 640 m elevation on rocky karst hills with a mean annual precipitation of 1529 mm and a mean annual temperature of 19.3°C. The sampling and on-site measurements were undertaken from November 2017 to January 2018 in the Malagasy site and July to August 2019 for the Chinese site, coinciding with the growing season at each study site.

Branch and leaf sampling

Leaf samples were obtained from a one-meter-long branch which was cut from the upper sun-exposed canopy for each of five to six individuals per species before 9 am. These branch samples were double-wrapped in plastic bags and transported to an on-site laboratory, re-cut underwater and rehydrated for 2–4 hours covered with plastic bags.

Imaging and measurement of leaf venation, stomatal traits and cross-sectional anatomy

The fresh leaf area of three fully developed leaves per individual was measured using a calibrated digital camera (Olympus E-PM2, China) for the Malagasy samples and a leaf area meter (LI-COR Li 3000C, USA) for the Chinese samples. These leaves were preserved in Formalin – Alcohol – Acetic acid fixation solution (10: 50: 5: distilled water 35) [50], and transported to the nearest research facility (University of Antananarivo, Madagascar for the tropical site, and Guangxi University, China for subtropical site). Minor vein density was measured from a 0.25 cm^2 section cut centrally in the leaf, avoiding major veins, which was digested in a 0.7% NaOH aqueous solution at 70°C until it became transparent [51], and when necessary, bleached, stained with a drop of 0.5% safranin for 5 min, washed with distilled water, and mounted on a microscope slide. Four images per leaf of approximately 1 mm^2 were taken at a resolution of 1.8 pixels·μm^{-1} (Leitz Orthoplan, Wetzlar, Germany) for the tropical site, and at 3.3 pixels·μm^{-1} (DM 3000 LED Wetzlar, Germany) for subtropical site, respectively. The calibration of both microscopes was verified using the same micrometer slide. Minor vein length, areole contours and length of free-ending veinlets (*FEV*) were manually drawn and measured using ImageJ (1.52p, National Institutes of Health, USA) [52]. The minor vein density (*VD*) and non-vein fraction (*nVF*) were calculated by dividing the vein length and non-vein area (areole area) respectively by the area of the field of view. *FEV* relative length was calculated by dividing *FEV* length by the total minor vein length.

For the measurement of stomatal traits, small paradermal sections of epidermis were prepared by hand, bleached, washed with distilled water, mounted on slides with glycerol, photographed with a digital

microscope (Tropical site; Subtropical site: DM 3000 LED Wetzlar, Germany), and measured for stomatal density (*SD*) and dimensions, that are, length (*L*), width (*W*), and pore length (*p*).

For the measurement of cross-sectional anatomy, transverse cross-sections were prepared by hand, double-stained with Safranin-Alcian blue, and imaged for measurement of leaf thickness, mesophyll thickness, the vertical distance between the minor vein and abaxial epidermis, and stomatal depth. Three images per leaf were taken using a 10× or 20× objective (C-mount 0.55x, respectively 3.3 and 6.6 pixels·µm^{-1}), depending on the leaf thickness, and, for three stomata, using a 100× objective (33.5 pixels·µm^{-1}) to measure the stomatal depth. The theoretical maximum stomatal conductance was calculated following Sack & Buckley (2016):

$$G_{smax} = bmds^{0.5} \ (1)$$

where, *b* and m are biophysical and morphological constants, respectively, and *d* and *s* represent stomatal density and stomatal size. $b = \frac{D}{v}$, where *D* is the diffusivity of water in the air and *v* is the molar air volume. $m = \frac{\pi c^2}{j^{0.5}(4hj+\pi c)}$, where *c* = the pore length to stomatal length ratio (*p*/*L*), *j* = the stomatal width to stomatal length ratio (*W*/*L*), *h* = the pore depth to stomatal width ratio (*l*/*W*).

Vein topological efficiency

Our approach to quantify vein topology efficiency (*VTE*) based on combining information of vein density with anatomical measurements of leaf cross-section images is illustrated in Fig. 6. For each leaf vein image, the edges around leaf veins were traced manually using a modified ImageJ polygon tool equipped with a drawing pad (Bosto 16 HDK, China), and the traced image was converted into a black (vein) and white (non-vein lamina) raster, from which the vein area was measured – hereafter referred to as the “real leaf” image. Total vein length was measured manually using a modified ImageJ polyline tool. Keeping the vein length and non-vein area fraction (*nVF*), the “real leaf” image was reconfigured into a simple square mosaic vein distribution image (hereafter “modeled leaf” image) with the exact same vein area fraction and vein length as the real leaf image.

To build the modelled leaf, we estimated the length of each grid segment (i.e., vein segment) (*S*) and the thickness of each grid segment (i.e., vein diameter) (Fig. 6-1B). Given that the vein density is the vein length per unit leaf area, the first step was to identify the leaf area associated with each grid segment (the area delimited by the broken green lines in Fig. 6-1B). Geometrically, this area represents half of whole areole. Therefore, *S* of the model can be calculated from *VD* of the real leaf using the Eq. (2):

$$VD = \frac{2S}{S^2} = 2 \times S^{-1} \text{, so, } S = 2 \times VD^{-1} \ (2)$$

Once the one-pixel thick grid was created, the *n* closest pixels were assigned as veins, where *n* is the number of vein pixels in the real leaf image. The thickness (*T*) of the vein on the model can also be calculated by solving the second-degree Eq. (2), the geometrical principle of this equation is detailed in

Supporting Information Note S1. The pixels representing veins were determined as being within a distance $T/2$ from the nearest vein center.

$\left(\frac{T}{S}\right)^2 - 2\frac{T}{S} + V_f = 0$ (3), thus, $\frac{T}{S} = 1 - \sqrt{1 - V_f}$, the other solution of the equation is unrealistic.

For both real and modeled images, the distance of each areole pixel to the nearest vein was computed using the *distance* function from the *raster* R-package [53]. Then, a buffer zone of 250 pixels from the edge of each image was deleted to remove the edge artifact. Indeed, areole pixels close to the edge were often farther from the nearest vein than they are in reality. The vein-to-lower epidermis distance was extracted from the cross-section image of the corresponding leaf, and the hypotenuse of the horizontal distance from the raster and the vein-to-epidermis distance from the leaf cross-section was calculated. To avoid the effect of outlier regions, we calculated the 95% quantile of the hypotenuse length (VS_{95}) for each image. The difference between VS_{95} calculated from the model-vein and its corresponding real-vein image divided by the VS_{95} of the real-vein image represents the influence of the native vein topology on the extraxylary pathlength, and is thus referred to as the vein topological efficiency (*VTE*; %). A positive *VTE* indicates that the arrangement of veins shortens the linear hydraulic pathlength through the mesophyll. Notably, this theoretical linear hydraulic pathlength is a proxy corresponding to the paths of the bulk flow of liquid water through and around mesophyll cells and diffusion of vapor in the airspaces [7]. We assumed the pathlength from vein to epidermis a proxy for flow to the stomata after Brodribb *et al*. (2007)Brodribb *et al.* (2007), without accounting for variation in stomatal density. We suggest that this assumption is justified given the typical correlation between stomatal density and vein density, as well as the conservation of stomatal arrangements in areoles [23].

Pressure-volume parameters

Two to four fully grown leaves were chosen from each individual and dehydrated on the bench while their leaf mass (10^{-3}g or 10^{-4}g digital balance; MT203T and MT204T, Shanghai, China) and water potential (Ψ_{leaf}) (Scholander pressure chamber; PMS 1505 D-EXP, Corvallis, OR, USA) were repetitively measured. Successive measurements were separated by a lag of 5 to 30 minutes to allow the leaves to dehydrate. Pressure-volume curves were constructed by plotting the reciprocal pressure ($1/\Psi_{leaf}$) against one minus relative water content (1 − *RWC*), where *RWC* was calculated as (fresh mass - oven-dry mass)/(saturated water mass - oven-dry mass) (Schulte & Hinckley 1985). Fresh leaf area of the species from the tropical and subtropical site was measured using a calibrated digital camera (Olympus E-PM2, China) and a leaf area meter (LI-COR Li 3000C, USA), respectively. Leaf mass was then determined by oven-drying the leaves at 70°C for at least 72 hours [51]. *RWC*-Ψ_{leaf} data were fitted with an exponential function after Schulte & Hinckley (1985) using the *nls* function in the *base* R-package [54]. The turgor loss point (*TLP*) is the water potential at the intersection between the non-linear and the non-linear portion of the curve ($1/\Psi_{leaf}$) = f(1 − *RWC*). The hydraulic capacitance C_1 (mol·MPa^{-1}·m^{-2}) was calculated following Blackman & Brodribb, (2011)Blackman & Brodribb, (2011):

$$C_1 = \frac{\Delta RWC}{\Delta WP} \times \frac{SWM}{LA \times M}$$

4

Where, ($\frac{\Delta RWC}{\Delta c\Psi_{\mathrm{leaf}}}$) ($MPa^{-1}$) was calculated from the slope of the initial non-linear portion of the pressure-volume curve, *SWM* (g) is the absolute saturated water mass, *LA* (m^2) is the fresh leaf area and *M* ($g.mol^{-1}$) is the water molar mass.

Testing the mechanism underlying VTE **and non-vein fraction**

To clarify the mechanistic association between *VTE* and non-vein fraction, we tested two hypotheses:

1. *All else being equal, gain in non-vein area is due to the absence of a connection between FEV tips and the vein at its opposite side.* We selected a leaf model with maximum redundancy and created a series of models with increasing number of *FEV*, from 1 to 13 *FEV*, as higher numbers of *FEV*s resulted in *VTE* > 11% which exceeded the range of the observed *VTE. VTE* and non-vein fraction of each model was calculated and plotted against empirical values.
2. *The gain in non-vein area is related to thinner veins along with increasing numbers of FEV*. A series of models with increasing number of *FEV* was created as above and the *VTE* of each element was calculated. For each element of the series, the thickness of the vein was set based on the empirical correlation between *VTE* and vein diameter. Then, their *VTE* and non-vein fraction was plotted against empirical values.

This series of modelled leaves were also used for analyzing the correlation between *VTE* and other leaf vein topological metrics in the published literature: the areole elongation rate and circularity using the LeafVeinCNN program [26,56] and the vein loopiness (mm^{-1}) and meshedness (unitless) was calculated using LeafGUI program [25,57].

Statistical analysis

Statistical analyses were performed using R 3.5.3 [54]. The leaves of two species from *Peperomia* genus were highly succulent, they were ouliers with extremely low vein density and long VS_{95} distance, and they were excluded from all correlation analyses. Correlations were fitted using the *sma* function from *smatr* package [58], and structural equation model (*SEM*) analyses were performed using the *lavaan* package [59]. Different hypothetical *SEM* models were fit and compared to evaluate the importance, placement, and effect size of different paths linking *FEV* properties, *VTE* and stomatal conductance. Key paths that were tested included direct linkage between vascular traits and *LMA* and/or stomatal conductance (e.g., *VTE* ◊ G_{Smax}), indirect linkage between vascular traits and stomatal conductance via biomass economics (e.g., *VTE* ◊ *LMA* ◊ G_{Smax}), as well as indirect linkage via pressure-volume parameters. Model fitting was simplified by manual step-wise path deletion beginning from the weakest path. At each step, the root mean square error of approximation (*RMSEa*) and the Akaike Information Criterion (*AIC*) were recorded.

The most parsimonious model (lowest *RMSEa* and AIC values) was selected. Phylogenetic information for the studied species was extracted from the GBOTB.extended database using the v.*Phylomaker* R-package [60], Blomberg's *K* phylogenetic signal and phylogenetic *ANOVA* for cross-habitat comparison were calculated using the *phytools* package [61]. Phylogenetic independent contrasts were calculated using the *ape* package [62]. Data were log transformed to normalize the distribution of residuals when required. The customizations made to the polygon and polyline tools in ImageJ, and all R-code, are available from the first author upon request.

Declarations

Competing interests: The authors declare no competing interests.

Acknowledgments

CKF was financially supported by the National Natural Science Foundation of China (31470469) and the Bagui Scholarship (C33600992001) of Guangxi Zhuang Autonomous Region. AA received funding from the China Scholarship Council. The authorization for the sample collection in Madagascar was issued by the 'Ministère de l'Environnement et du Développement Durable' – Madagascar – Research authorization: 262/17-MEEF/SG/DGF/DSAP/SCB.Re of 2017, 24th October. We are grateful to the Madagascar National Park MNP, the institution managing the Anjanaharibe-Sud Nature Reserve, and Mr. Jo, the forest ranger who served as our field guide in Madagascar.

Author contributions

AA and KFC designed the study. AA, KFC, YZL, SMG and LS wrote the manuscript. AA and RT collected the samples and analyzed the species from Madagascar. AA, MYN and SDZ analyzed the species from China. The image and data analyses were done by AA. All authors have reviewed and approved the manuscript.

References

1. McCulloh, K. A., Sperry, J. S. & Adler, F. R. Water transport in plants obeys Murray's law. Nature **421**, 939–942 (2003).
2. Anfodillo, T., Carraro, V., Carrer, M., Fior, C. & Rossi, S. Convergent tapering of xylem conduits in different woody species. New Phytol **169**, 279–290 (2006).
3. Olson, M. E. *et al.* Universal hydraulics of the flowering plants: vessel diameter scales with stem length across angiosperm lineages, habits and climates. Ecol. Lett. **17**, 988–997 (2014).
4. Sack, L. & Frole, K. Leaf structural diversity is related to hydraulic capacity in tropical rain forest trees. Ecology **87**, 483–491 (2006).

5. Brodribb, T. J., Feild, T. & Jordan, G. J. Leaf maximum photosynthetic rate and venation are linked by hydraulics. Plant Physiol. **144**, 1890–1898 (2007).
6. Brodribb, T. J. Xylem hydraulic physiology: The functional backbone of terrestrial plant productivity. Plant Science **177**, 245–251 (2009).
7. Buckley, T. N., John, G. P., Scoffoni, C. & Sack, L. How does leaf anatomy influence water transport outside the xylem? Plant Physiol. **168**, 1616–1635 (2015).
8. Cochard, H., Nardini, A. & Coll, L. Hydraulic architecture of leaf blades: where is the main resistance? Plant Cell Environ **27**, 1257–1267 (2004).
9. Sack, L. & Holbrook, N. Leaf hydraulics. Annu. Rev. Plant Biol **57**, 361–81 (2006).
10. Scoffoni, C. *et al.* Outside-xylem vulnerability, not xylem embolism, controls leaf hydraulic decline during dehydration. Plant Physiol. **173**, 1197–1210 (2017).
11. Liu, X.-R. *et al.* Water transport from stem to stomata: the coordination of hydraulic and gas exchange traits across 33 subtropical woody species. Tree Physiol **39**, 1665–1674 (2019).
12. Sack, L. & Scoffoni, C. Leaf venation: structure, function, development, evolution, ecology and applications in the past, present and future. New Phytol **198**, 983–1000 (2013).
13. Beerling, D. J. & Franks, P. J. The hidden cost of transpiration. Nature **464**, 495–496 (2010).
14. McKown, A. D., Cochard, H. & Sack, L. Decoding leaf hydraulics with a spatially explicit model: principles of venation architecture and implications for its evolution. Am. Nat **175**, 447–460 (2010).
15. Koçillari, L. *et al.* The widened pipe model of plant hydraulic evolution. *Proc. Natl. Acad. Sci. U.S.A.* **118**, e2100314118 (2021).
16. Noblin, X. *et al.* Optimal vein density in artificial and real leaves. *Proc. Natl. Acad. Sci. U.S.A.* **105**, 9140–9144 (2008).
17. de Boer, H. J., Eppinga, M. B., Wassen, M. J. & Dekker, S. C. A critical transition in leaf evolution facilitated the Cretaceous angiosperm revolution. Nat Commun **3**, 1221–1232 (2012).
18. Zwieniecki, M. A. & Boyce, C. Evolution of a unique anatomical precision in angiosperm leaf venation lifts constraints on vascular plant ecology. Proc R Soc Lond B Biol Sci **281**, 20132829–20132829 (2014).
19. John, G. P. *et al.* The anatomical and compositional basis of leaf mass per area. Ecol Lett **20**, 412–425 (2017).
20. Sack, L. *et al.* Leaf mass per area is independent of vein length per area: avoiding pitfalls when modelling phenotypic integration (reply to Blonder et al. 2014). *J Exp Bot* **65**, 5115–5123 (2014).
21. Chapin, F. S., Matson, P. A. & Vitousek, P. M. *Principles of terrestrial ecosystem ecology*. (Springer New York, 2011). doi:10.1007/978-1-4419-9504-9.
22. Katifori, E. The transport network of a leaf. C R Phys **19**, 244–252 (2018).
23. Fiorin, L., Brodribb, T. J. & Anfodillo, T. Transport efficiency through uniformity: organization of veins and stomata in angiosperm leaves. New Phytol **209**, 216–227 (2016).

24. Blonder, B. *et al.* Structural and defensive roles of angiosperm leaf venation network reticulation across an Andes–Amazon elevation gradient. J Ecol **106**, 1683–1699 (2018).
25. Price, C. A. & Weitz, J. S. Costs and benefits of reticulate leaf venation. BMC Plant Biol **14**, 234 (2014).
26. Blonder, B. *et al.* Linking functional traits to multiscale statistics of leaf venation networks. New Phytol **228**, nph.16830 (2020).
27. Brodribb, T., Feild, T. & Sack, L. Viewing leaf structure and evolution from a hydraulic perspective. Funct. Plant Biol. **37**, 488–498 (2010).
28. Sack, L. *et al.* How do leaf veins influence the worldwide leaf economic spectrum? Review and synthesis. J Exp Bot **64**, 4053–4080 (2013).
29. McElwain, J. C., Yiotis, C. & Lawson, T. Using modern plant trait relationships between observed and theoretical maximum stomatal conductance and vein density to examine patterns of plant macroevolution. New Phytol **209**, 94–103 (2016).
30. Scoffoni, C. *et al.* Hydraulic basis for the evolution of photosynthetic productivity. Nat. Plants **2**, 16072 (2016).
31. Zhao, W.-L., Chen, Y.-J., Brodribb, T. J. & Cao, K.-F. Weak co-ordination between vein and stomatal densities in 105 angiosperm tree species along altitudinal gradients in Southwest China. Funct. Plant Biol. **43**, 1126 (2016).
32. Gleason, S. M. *et al.* Weak coordination among petiole, leaf, vein, and gas-exchange traits across Australian angiosperm species and its possible implications. Ecol Evol **6**, 267–278 (2016).
33. Xiong, D. L. & Flexas, J. From one side to two sides: the effects of stomatal distribution on photosynthesis. New Phytol **228**, 1754–1766 (2020).
34. de Boer, H. J. *et al.* Apparent overinvestment in leaf venation relaxes leaf morphological constraints on photosynthesis in arid habitats. Plant Physiol **172**, 2286–2299 (2016).
35. Rodriguez-Dominguez, C. M. & Brodribb, T. J. Declining root water transport drives stomatal closure in olive under moderate water stress. New Phytol **225**, 126–134 (2020).
36. Carminati, A. *et al.* Stomatal closure prevents the drop in soil water potential around roots. New Phytol **226**, 1541–1543 (2020).
37. Li, L., Ma, Z., Niinemets, Ü. & Guo, D. Three key sub-leaf modules and the diversity of leaf designs. Front. Plant Sci. **8**, 1–8 (2017).
38. Griffith, D. M., Quigley, K. M. & Anderson, T. M. Leaf thickness controls variation in leaf mass per area (LMA) among grazing-adapted grasses in Serengeti. Oecologia **181**, 1035–1040 (2016).
39. Alonso-Forn, D. *et al.* Revisiting the functional basis of sclerophylly within the leaf economics spectrum of oaks: Different roads to Rome. Curr Forestry Rep **6**, 260–281 (2020).
40. Sperry, J. S. Evolution of water transport and xylem structure. International Journal of Plant Sciences **164**, S115–S127 (2003).

41. Zhang, Y. *et al.* Xylem conduit deformation across vascular plants: an evolutionary spandrel or protective valve? New Phytol (2022) doi:10.1111/nph.18584.
42. Ding, Y.-T., Zhang, Y.-X., Zheng, Q.-S. & Tyree, M. T. Pressure-volume curves: revisiting the impact of negative turgor during cell collapse by literature review and simulations of cell micromechanics. New Phytol **203**, 378–387 (2014).
43. Fu, X. *et al.* Coordination and trade-offs between leaf and stem hydraulic traits and stomatal regulation along a spectrum of isohydry to anisohydry. Plant Cell Environ **42**, 2245–2258 (2019).
44. Wright, I. J. *et al.* The worldwide leaf economics spectrum. Nature **428**, 821–827 (2004).
45. Gorné, L. D. *et al.* The acquisitive–conservative axis of leaf trait variation emerges even in homogeneous environments. Ann. Bot **129**, 709–722 (2020).
46. Feild, T. *et al.* Fossil evidence of Cretaceous escalation in angiosperm leaf vein evolution. Proc Natl Acad Sci USA **108**, 8363–8366 (2011).
47. Schatz, G. E., Lowry, P. P. & Ramisamihantanirina, A. Takhtajania perrieri rediscovered. Nature **391**, 133–134 (1998).
48. Goodman, S. *A floral and faunal inventory of the Réserve spéciale d'Anjanaharibe-Sud, Madagascar*. (Field Museum of Natural History, 1998). doi:10.5962/bhl.title.3148.
49. Hudson, P. J., Razanatsoa, J. & Feild, T. Early vessel evolution and the diversification of wood function: Insights from Malagasy Canellales. Am. J. Bot. **97**, 80–93 (2010).
50. Ruzin, S. E. *Plant microtechnique and microscopy*. (Oxford University Press, 1999).
51. Perez-Harguindeguy, N. *et al.* New handbook for standardised measurement of plant functional traits worldwide. Aust. J. Bot **61**, 167–234 (2013).
52. Rueden, C. T. *et al.* ImageJ2: ImageJ for the next generation of scientific image data. BMC Bioinform **18**, 529 (2017).
53. Hijmans, R. & van Etten, J. Raster: Geographic data analysis and modeling. R Package Version **517**, 2–12 (2014).
54. R Core Team. R: A language and environment for statistical computing. (2019).
55. Blackman, C. J. & Brodribb, T. J. Two measures of leaf capacitance: insights into the water transport pathway and hydraulic conductance in leaves. Funct. Plant Biol. **38**, 118 (2011).
56. Xu, H., Blonder, B., Jodra, M., Malhi, Y. & Fricker, M. Automated and accurate segmentation of leaf venation networks via deep learning. New Phytol **229**, 631–648 (2021).
57. Price, C. A., Symonova, O., Mileyko, Y., Hilley, T. & Weitz, J. S. Leaf extraction and analysis framework graphical user interface: segmenting and analyzing the structure of leaf veins and areoles. Plant Physiol **155**, 236–245 (2011).
58. Warton, D. I., Duursma, R. A., Falster, D. S. & Taskinen, S. smatr 3- an R package for estimation and inference about allometric lines: The smatr 3 - an R package. Methods Ecol. Evol. **3**, 257–259 (2012).
59. Rosseel, Y. lavaan: An R package for structural equation modeling. J. Stat. Softw **48**, 1–36 (2012).

60. Jin, Y. & Qian, H. V.PhyloMaker: an R package that can generate very large phylogenies for vascular plants. Ecography **42**, 1353–1359 (2019).
61. Revell, L. J. phytools: an R package for phylogenetic comparative biology (and other things): phytools: R package. Methods Ecol. Evol. **3**, 217–223 (2012).
62. Paradis, E. & Schliep, K. ape 5.0: an environment for modern phylogenetics and evolutionary analyses in R. *Bioinformatics* **35**, 526–528 (2019).

Figures

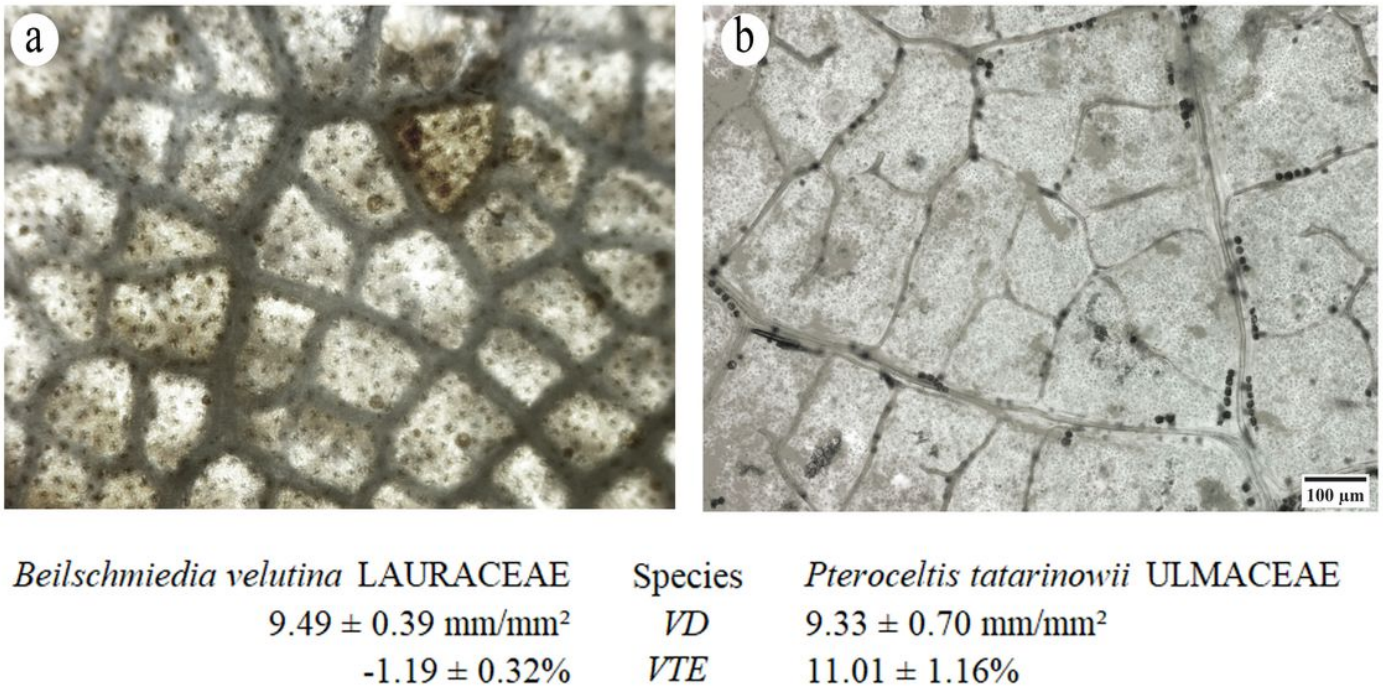

Figure 1

Micrographs showing leaf veins for the species with the lowest and highest vein topological efficiency (VTE), which had similar vein density.

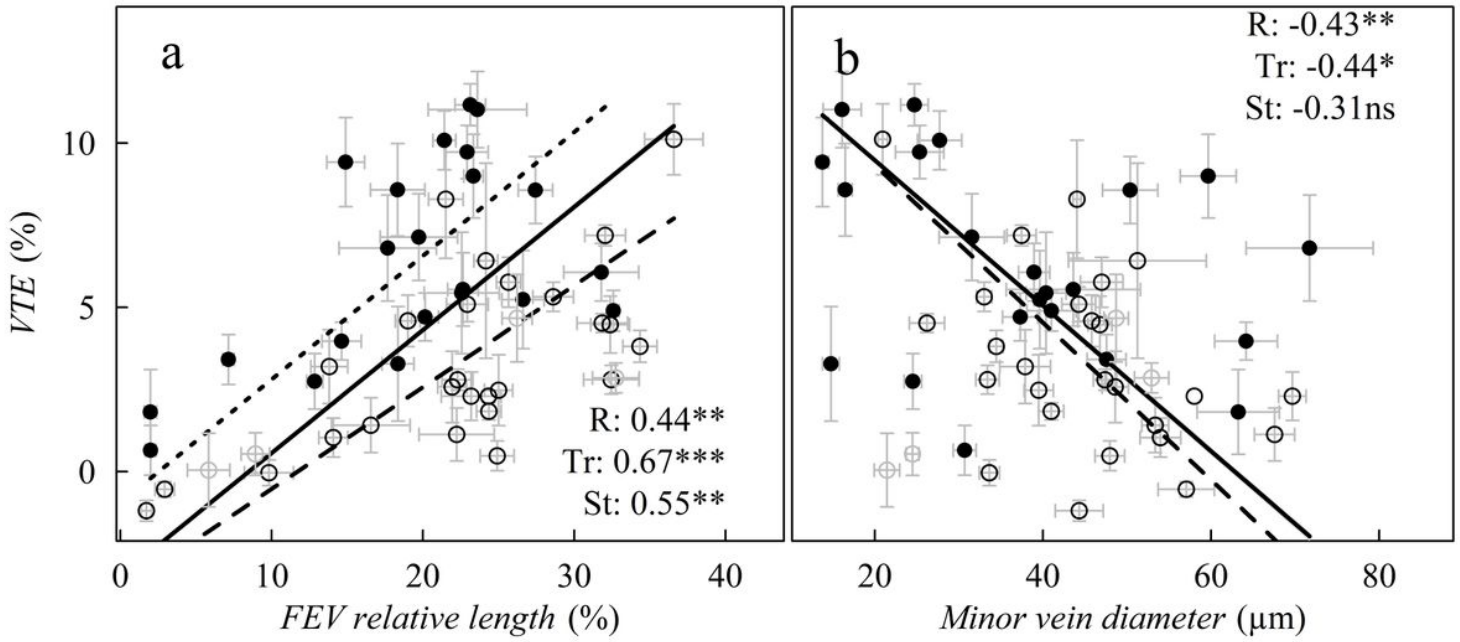

Figure 2

Contribution of free end veinlets (FEV) to vein topological efficiency (*VTE*), and correlation between vein topological efficiency (*VTE*) and average minor vein diameter. Open circles and dashed lines denote species from the tropical site (Tr), and filled circles and dotted line denote species from the subtropical site (St). Data are mean values and error bars are standard errors. The significance of each correlation is represented by: ***: $p<0.001$, **: $0.001<p<0.01$, *:$0.01<p<0.05$ and “ns” for non-significant correlations.

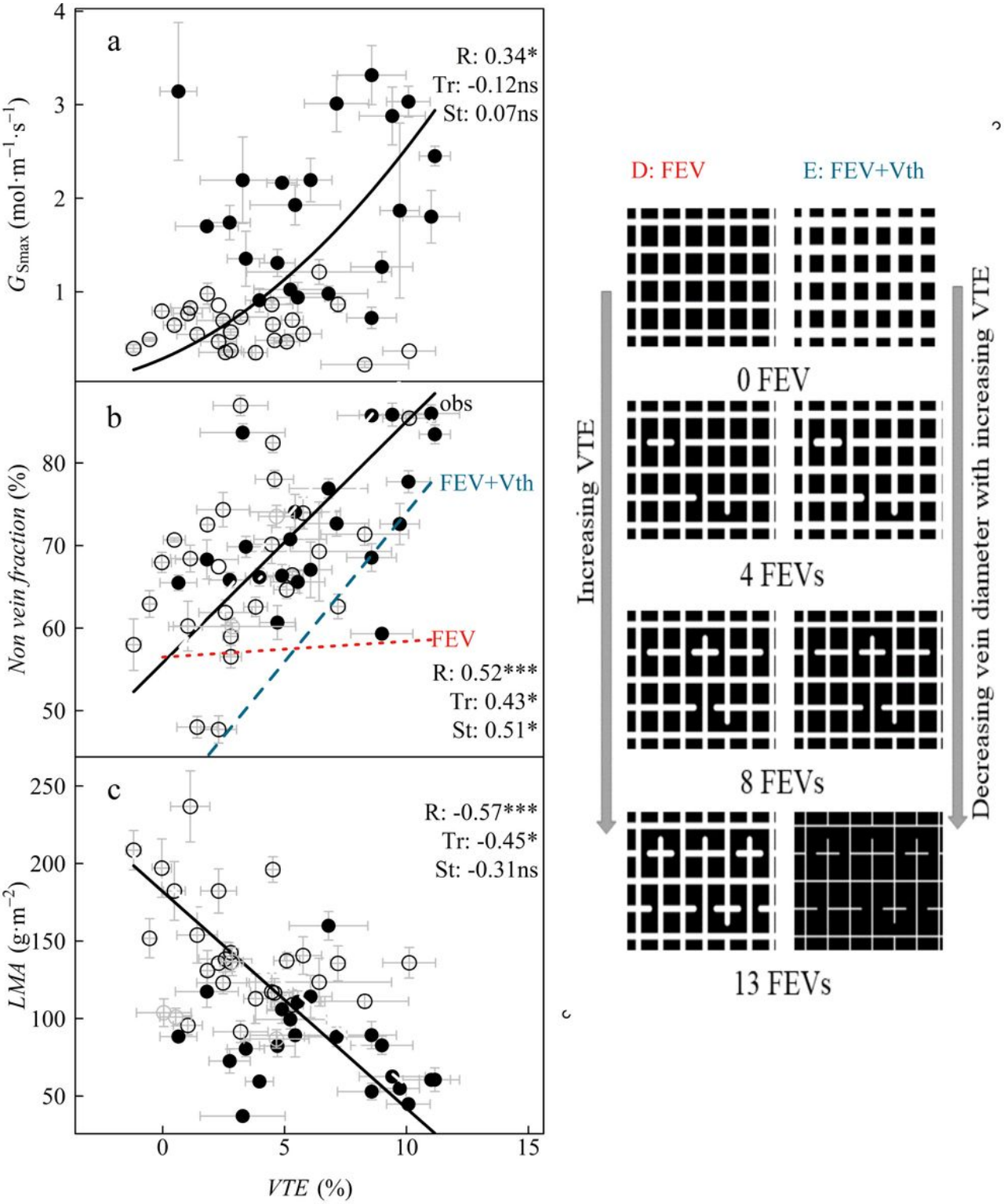

Figure 3

Associations of vein topological efficiency (*VTE*) with (a) the theoretical maximum stomatal conductance (G_{smax}), (b) non-vein area fraction, and (c) leaf mass per area (*LMA*). (d) and (e) illustrate samples of a series of model with increasing free-ending veinlet (*FEV* density - increasing *VTE* – with constant and decreasing minor vein diameter (*Vth*), respectively. In the panel (b), *obs* (black) is the measured non-vein fraction, the red dashed line labelled "*FEV*" is *nVF* calculated from the area that was supposed to link the

tip of the *FEVs* and the vein at its opposite side, the blue dotted line labelled "*FEV+ Vth*" is *nVF* increase driven by the correlation between *VTE* and minor vein diameter. The open circles are the species from the tropical site (*Tr*) and the filled points are the subtropical site (*St*). Data are mean values and error bars are the standard errors. The significance of each correlation is represented by: ***: p<0.001, *:0.01<p<0.05 and "ns" for non-significant correlations.

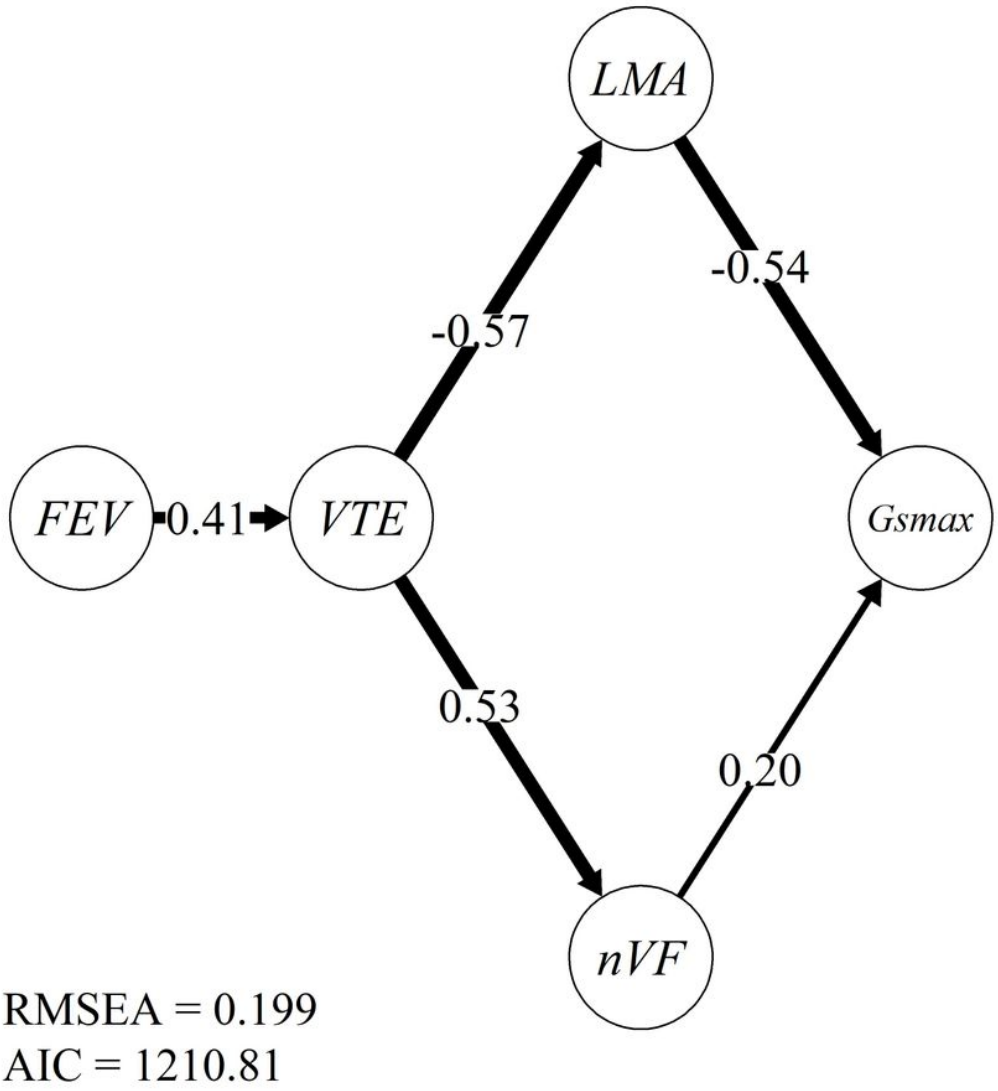

Figure 4

Structural equation model linking free-end veinlet relative length (*FEV*), vein topological efficiency (*VTE*) and stomatal conductance (G_{smax}) via space (non-vein fraction *nVF*) and biomass economics (*LMA*). Labeled connections represent standardized slope coefficients.

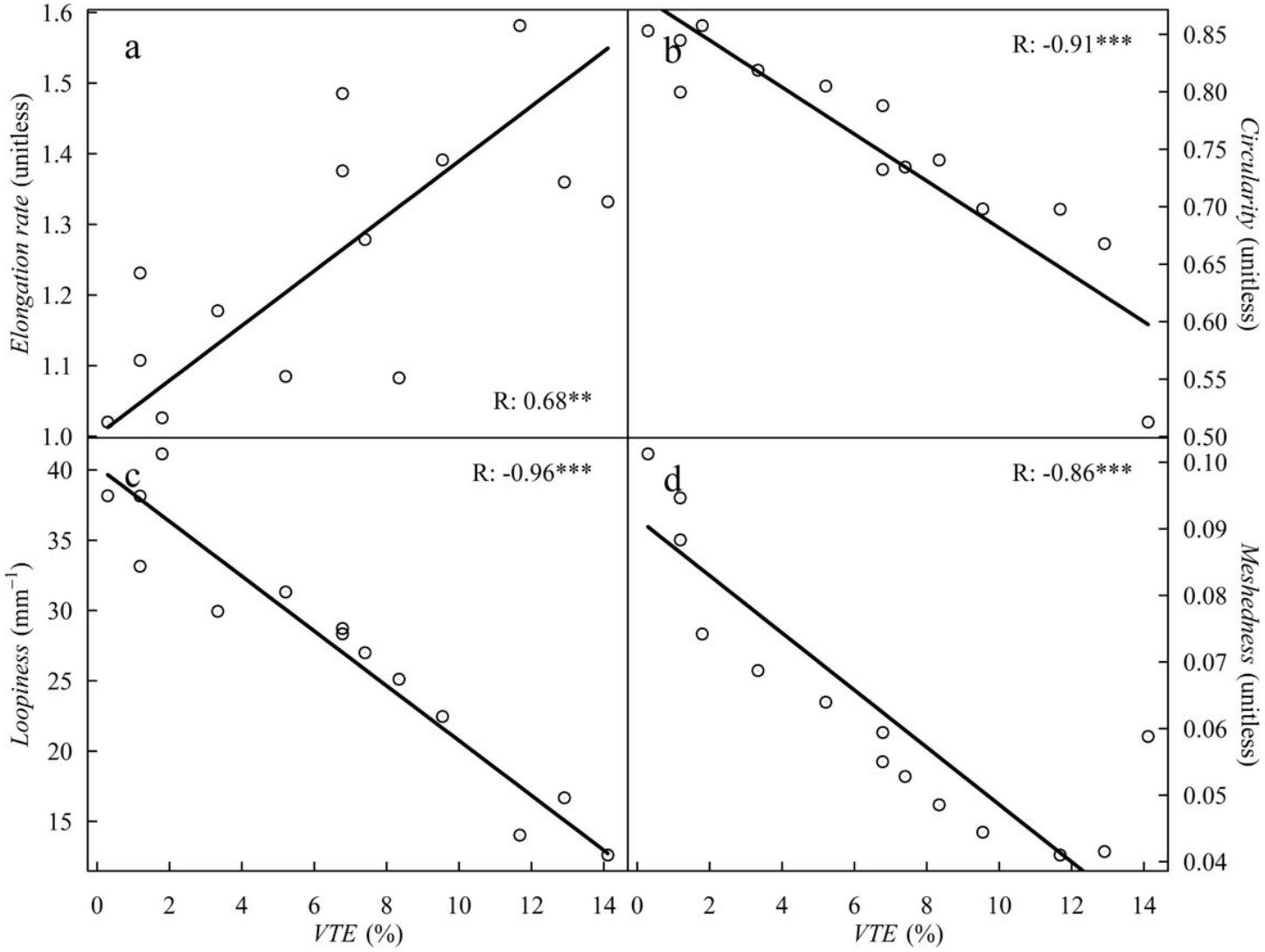

Figure 5

Correlations between vein topological efficiency (*VTE*) and other metrics of vein topology across model leaves with increasing free-end veinlet numbers. These metrics include the areole elongation rate and circularity, reported by Blonder *et al.* (2020) and vein loopiness and meshedness, reported by Price & Weitz (2014). The significance of each correlation is represented by: ***: p<0.001, **: 0.001<p<0.01.

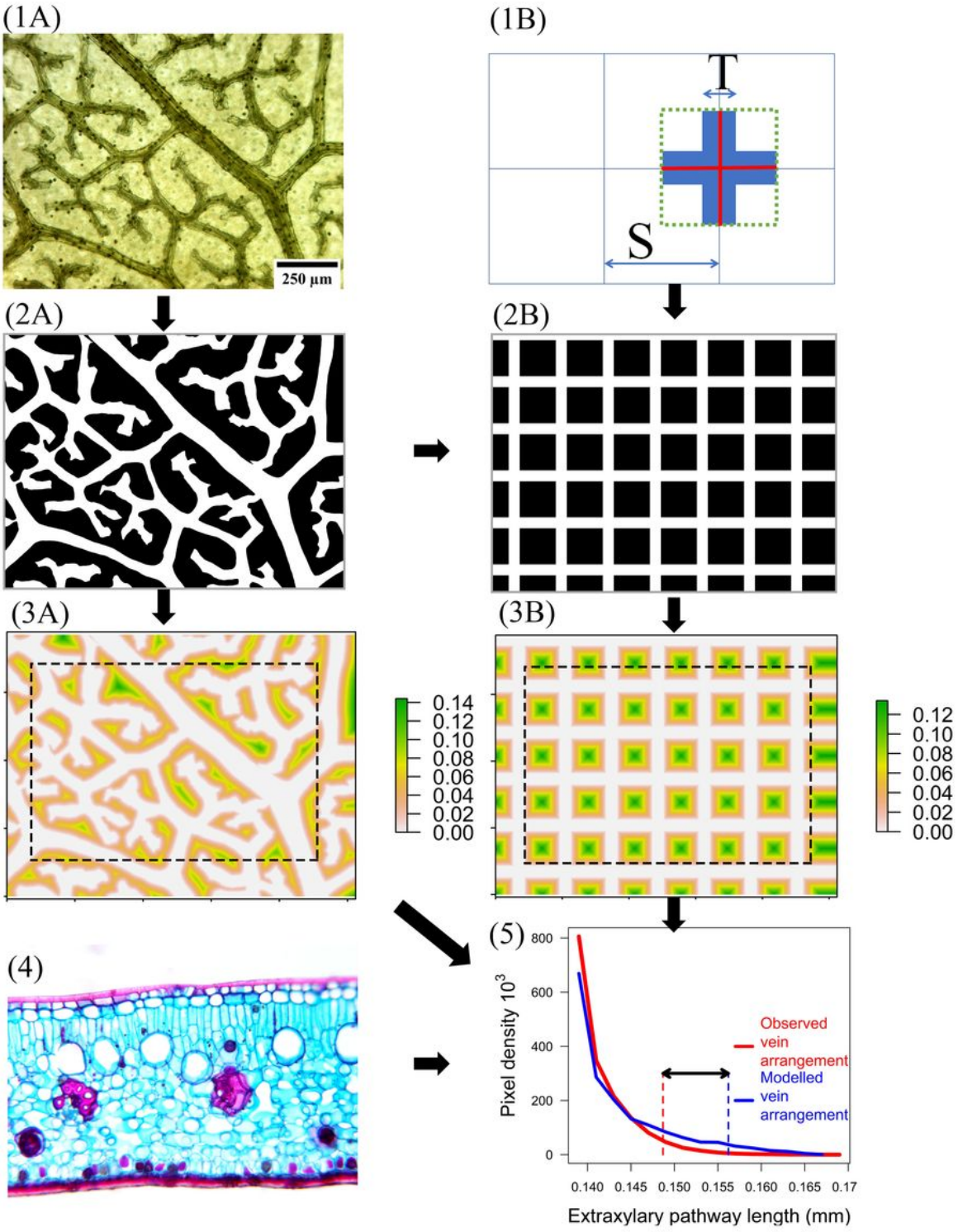

Figure 6

Measurements of venation characteristics and calculation of the vein topological efficiency (*VTE*).

Supplementary Files

This is a list of supplementary files associated with this preprint. Click to download.

- SupportingInformation20221205nolink.docx